UtilitasMathematica

ISSN 0315-3681 Volume 122 (2), 2025

An alternate approach for Influence Coefficients computation for Unbalance identification in a multi disc rotor system

Dinesh Kumar Pasi

Associate Professor, Department of Mechanical Engineering, Shri G. S. Institute of Technology and Science, Indore. India

dkpasi25@gmail.com

Abstract

This work introduces an Influence Coefficient-based approach for identifying imbalances in a multi-disc rotor system. A method was developed that employs the measurement of imbalance response at specified locations and computes the effect coefficient using the finite element model of the rotor system during the unbalance identification process. Experiments on a rotor test rig have shown that the method works well for balancing multi-disc rotor systems. Using influence coefficients from a finite element model in the imbalance response identification procedure means that a long experimental trial run is not needed. It is very important to make sure that the finite element model of the rotor system is correct in order to find the source of the imbalance. The method may look at how unevenly the rotor shaft system is spread out. The obtained influence coefficients from the updated finite element model of the rotor system are used to create an Influence Coefficient matrix. The experimental rotor system was made unbalanced at certain angles, and the resulting vibrations were recorded at certain measurement sites to make the response vector. So, the algorithm finds the imbalance in the rotor system by using the unbalance response values at the measurement points and the effect coefficient matrix. The suggested solution is thought to work well for balancing systems with many discs.

Keywords- Unbalance Response, Influence Coefficient Matrix, Unbalance Identification, Response Vector.

1 Introduction

Unbalance serves as the principal cause of excitation in rotating machines, which, if not promptly rectified, may result in other defects inside the machines [1]. The eccentricity of the rotor mass induces a main spin synchronous excitation in the rotor, the strength of which increases with the shaft's rotational speed. The equilibrium state deteriorates during operation due to several factors, such as dirt collection, corrosion, erosion, and particle impact [2]. It is crucial that during acceleration and at operational speed, the vibration levels remain below safe and acceptable ranges; exceeding these limits necessitates balance [3]. The predominant failure mechanism of a rotor is lateral vibration, which mostly arises from an imbalance inside the rotor [4]. The balancing of rotating machines is a standard procedure to mitigate vibrations caused by unbalanced forces; hence, quick diagnosis and correction of imbalance in these machines is crucial [1, 5] . Numerous techniques have been established for the diagnosis and correction of imbalance in rotating machinery. The enhancement of current techniques and the

creation of novel approaches for imbalance diagnosis and balancing remain a dynamic and promising research domain [6]. Shrivastava and Mohanty (2019) introduced a combined state input estimation method for imbalance identification, whereby the estimated unbalance force is juxtaposed with the unbalance force derived from the mathematical model to ascertain the unbalance parameter using the least squares methodology. A technique for identifying unbalance and shaft bow was introduced, using correlation analysis and the system equivalent reduction and expansion process (SEREP) for a two-disc rotor system [5]. Yao, et al. (2018) suggested a modal expansion and optimization-based approach for identifying the imbalance parameter in a single disc rotor bearing system.

Rotors may be classified into two major categories: stiff rotor systems and flexible rotor systems. A rotor is considered rigid if it can function at any speed, other than for its balanced speed, without a noticeable rise in vibration levels. The flexible rotors function well at their balancing speed [7]. Imbalances in stiff rotors may be rectified in any two arbitrarily selected planes. Balancing a flexible rotor is far more challenging than balancing a rigid rotor on the balancing machine, since the support stiffness influences the deflected form. Rotors may be balanced using specialised balancing devices or by in-situ/field balancing techniques [8].

In 1870 Henry Martinson first ever balancing machine was patented [9] and before that balancing was not known or needed in any industry. Even after the development of balancing machine a trial and error method was popular for balancing in the as late as 1920 [9, 10]. In-situ/field balancing involves balancing a rotor in its own bearings and support structure, rather than in a balancing machine. The conventional field balancing methods are classified into three categories, namely (i) the modal balancing method, (ii) the influence coefficient method and (iii) the unified approach method [9, 11]. These approaches need precise instrumentation for detecting imbalance in the machines, followed by the implementation of suitable balancing procedures. The influence coefficient technique entails monitoring response and phase angles throughout the computation of influence coefficients during initial and trial runs. The collected information about the system is used to calculate the balancing masses and their respective angles. Nonetheless, a significant drawback of this strategy is its need for several test iterations. The modal balancing approach, conversely, needs fewer test runs. The modal balancing approach utilises previous knowledge of the system's inherent frequencies and mode shapes to compute orthogonal weight sets for test runs and balancing [12]. However, the approach is limited in its capacity to balance rotors with complex and speed-dependent eigenfunctions, especially for rotors supported by hydrodynamic journal bearings, owing to the lack of an orthogonal weight set [13]. After analysing the pros and cons of the modal and influence coefficient methods, a unified strategy to balancing flexible rotors was devised. [14-16].

Various other approaches have also been discovered for unbalance identification and balancing of rotating machines. Run-up and run-down test data of the rotating machine gives useful information about the system. Sinha, et al. (2004) proposed estimation of unbalance of a rotating machine from a single run-down. Later on, the work was extended for the estimation of unbalance and misalignment simultaneously using the single run down data as well as Influence Coefficient analysis [17].

A lot of focus has been on model-based defect detection approaches as of late. In model-based approaches, however, the precision of the numerical model is crucial [18]. A technique for identifying and balancing rotor systems based on the Influence Coefficient of imbalance response is presented in this paper. A survey of methods for detecting defects using models is given by Lees, et al. (2009). When errors are present, the system's dynamic behaviour changes. The healthy system model takes this change into account by applying comparable loads. Applying imaginary pressures and moments to the model of a healthy system causes it to react dynamically in the same way that the real damaged system would under real-world conditions. As a mathematical representation, the Fault Model shows equal loads [18]. To handle imbalance and misalignment in steady-state situations, Jalan and Mohanty (2009) Jalan and Mohanty (2009) presented a residual generation method that is combined with model-based fault diagnostics for rotor bearing systems. In order to detect unbalance and rotor cracks, a similar fault model has been used [21, 22]. Sudhakar and Sekhar (2010) employed analogous loads minimisation and vibration minimisation techniques for defect identification, achieving minimal error by sensing transverse vibration at a single spot. In order to find the unbalanced mass, Zhang, et al. (2010) presented the whole-beat correlation method for fully balancing a dual-rotor system with a small speed disparity.

Machine learning techniques also find their applications in machinery fault diagnosis. Using model data to train an Artificial Neural Network (ANN), Furtado, et al. (2005) combined ANN with model-based defect diagnosis. Because the machine's vibration response varies with speed, fault diagnosis in variable speed equipment presents unique issues. When using conventional methods of condition monitoring, the vibration response might be misleading since it varies with changes in speed. McBain and Timusk (2009) used statistical approaches to solve the problem of defect prediction in variable speed equipment by segmenting the vibration response into speed bins with a restricted range of speeds. J K Sinha endeavoured to decrease the quantity of sensors per pedestal bearing by improving computing techniques in signal processing [27, 28]. The authors amalgamated data from all sensors within the frequency domain to generate a composite spectrum of the machine and proficiently analysed vibration data by computing higher-order spectra to detect flaws. Chatzisavvas and Dohnal (2014) applied least angle regression (LAR) technique for equivalent load method on sparse vibration measurement for unbalance identification.

Yao, et al. (2018) demonstrated that the identification and optimisation strategy for the combined modal expansion/inverse problem approach yields more precise predictions than those produced by the pure modal expansion method. Shrivastava and Mohanty (2019) Jalan proposed a method for estimating unbalanced forces through a joint-input state estimation technique, which was validated via numerical simulations and experimental observations. Chouksey, et al. (2013) utilised a corrected finite element model of a singular disc rotor system to rectify the imbalance in the system's single disc. To calculate the balancing mass, the authors minimised the rotor vibrations using the imbalance response Influence Coefficient of the disc. Unbalanced rotor systems have not yet had the Influence Coefficient -based method expanded to handle their detection. For machine balancing purposes, this study expands the Influence Coefficient-based

approach to imbalance detection in multi-disc rotor systems. It should be mentioned that this method might potentially help find imbalances on the rotor-shaft. The next part describes the theoretical foundation for the same.

2 Theoretical basis

In this part, the algebraic foundation, modelling assumptions, equations of motion, and modal analysis equations are laid forth, along with the imbalance detection technique.

2.1 Equations of Motion

The rotor-shaft system is modelled using the finite element approach in this particular piece of work. In order to simulate the rotor shaft, two-noded beam elements are utilised, whereas point mass/inertia elements are utilised to represent the rotor discs. In addition to taking into account gyroscopic effects, the model takes into account the flexibility of the shaft and bearings, as well as the rotary and translational inertia of the discs and the shaft. Figure 1 may be referred for an illustration of the degrees of freedom that were taken into consideration for the i^{th} beam element.

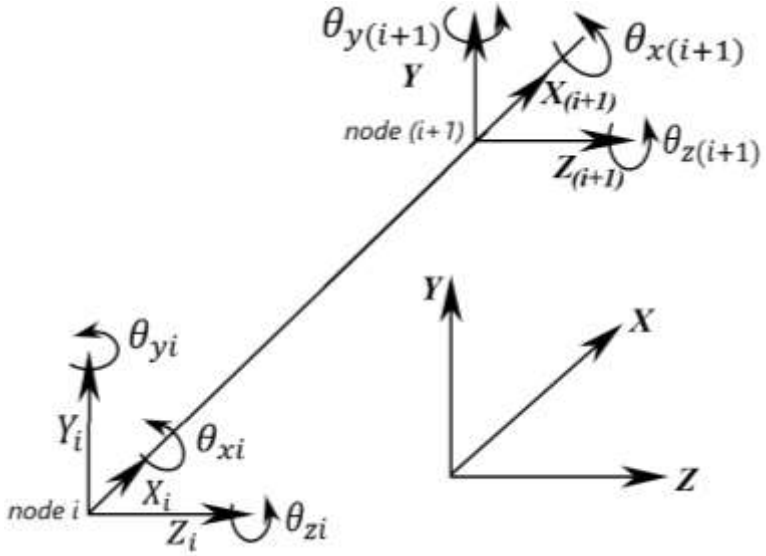

Figure 1 Nodal degrees of freedom and the i^{th} element

Equations of motion for the rotor shaft system may be stated as follows, with *N* degrees of freedom and the boundary conditions incorporated into the equations:

$$\mathbf{M}\ddot{\mathbf{q}}(t)+\mathbf{C}\dot{\mathbf{q}}(t)+\mathbf{K}\mathbf{q}(t)=\mathbf{f}(t) \qquad \text{Eqn. 1}$$

$$\text{where} \quad \mathbf{M}=\mathbf{M}_{trs}+\mathbf{M}_{rot}; \quad \mathbf{C}=[-\Omega\,\mathbf{G}+\mathbf{C}_{brg}] \; and \; \mathbf{K}=[\mathbf{K}_{brg}+\mathbf{K}_{sh}] \qquad \text{Eqn. 2}$$

The equation (1) uses symbols '$\mathbf{M}$' stands for mass matrix which includes translational mass components due to translation ($\mathbf{M}_{trs}$) and rotary inertia effect is taken care by the symbol ($\mathbf{M}_{rot}$). The notation $\mathbf{C}$ is used for representing non-symmetric matrix coefficient of the velocity vector in which skew-symmetric gyroscopic matrix ($\mathbf{G}$) and the damping matrix due to journal bearing (C_{brg}) are incorporated. The matrix coefficient of the displacement vector is represented by '$\mathbf{K}$' which has two elements first one is

stiffness matrix due to the bearings ($\mathbf{K}_{brg}$) and other one is stiffness matrix due to shaft flexibility ($\mathbf{K}_{sh}$). The size of all the matrices are of $N \times N$. The symbol 'Ω' stands for rotor spin speed in radian /second. Time is represented by 't' and '˙' is used to indicate derivative of time. Within the scope of this work, the matrices are represented by capital letters and bold letters, while the row and column vectors and scalars are represented by small bold and italic letters, respectively.

2.2 Unbalance identification using Influence Coefficient Matrix

In the next section, the generalised version of the Influence Coefficient-based technique to identifying imbalance is presented. The estimation of the rotor's imbalance is accomplished by the use of model-based Influence Coefficients in conjunction with the utilisation of measured unbalance reactions at specific points. In accordance with the information presented in the preceding section, the Influence Coefficient and the matrix that corresponds to it are estimated by using the finite element model of the rotor system.

It is possible to define the influence coefficient as the imbalance reaction at point *i* (where *i* = 1, 2, 3, 4…m) in a given direction owing to the unit rotational unbalance force at point *j* (where *j* =1, 2, 3, 4…n). The influence coefficient is represented by s_{ij}, and it is calculated using the finite element model (FE). In this equation, the variables m and n stand for the number of measurement points and the locations of the unbalanced points, respectively.

A generalised version of the matrix representing the influence coefficient is being written;

$$\mathbf{S} = \begin{bmatrix} s_{11} & s_{12} & s_{13} & - & - & s_{1n} \\ s_{21} & s_{22} & s_{23} & - & - & s_{2n} \\ s_{31} & s_{32} & s_{33} & - & - & s_{3n} \\ - & - & - & - & - & - \\ - & - & - & - & - & - \\ s_{m1} & s_{m2} & s_{m3} & - & - & s_{mn} \end{bmatrix} \qquad \text{Eqn. 3}$$

Unbalance detection is accomplished by the use of the measured unbalance response at specific point on the shaft in this study. Equation (4) is the expression of the response vector '**y**' that has been measured. Equation (5) provides the imbalance force vector '**f**' that corresponds to the number of unbalance sites there are when '*n*' of them are taken into consideration.

$$\mathbf{y} = \begin{Bmatrix} y_1 \\ y_2 \\ y_3 \\ - \\ - \\ y_m \end{Bmatrix} \qquad \text{Eqn. 4}$$

$$\mathbf{f} = \begin{Bmatrix} f_1 \\ f_2 \\ f_3 \\ - \\ - \\ f_n \end{Bmatrix} \qquad \text{Eqn. 5}$$

Following the computation of the Influence Coefficient matrix **S** and the acquisition of the observed imbalance response vector **y**, it is possible to determine the specific unbalance that exists inside the rotor system. The relationship between the Influence Coefficient matrix **S**, the reaction vector **y**, and the imbalance force vector **f** is represented by the equation known as Equation (6).

$$\mathbf{S \times f = y} \qquad \text{Eqn. 6}$$

Writing the Equation 6 to estimate unbalance force vector as Equation 7 below;

$$\mathbf{f = S^{-1} \times y} \qquad \text{Eqn. 7}$$

3 Methodology

Figure 2 shows the flow chart of the methodology for unbalance identification. It shows first formation of Influence Coefficient matrix using the finite element model. In the next step, unbalance response is measured on the machine. Finally, the vector of unbalance is computed using the algorithm and balancing procedure performed [31]. The experimental work will be followed by numerical simulation to illustrate the process.

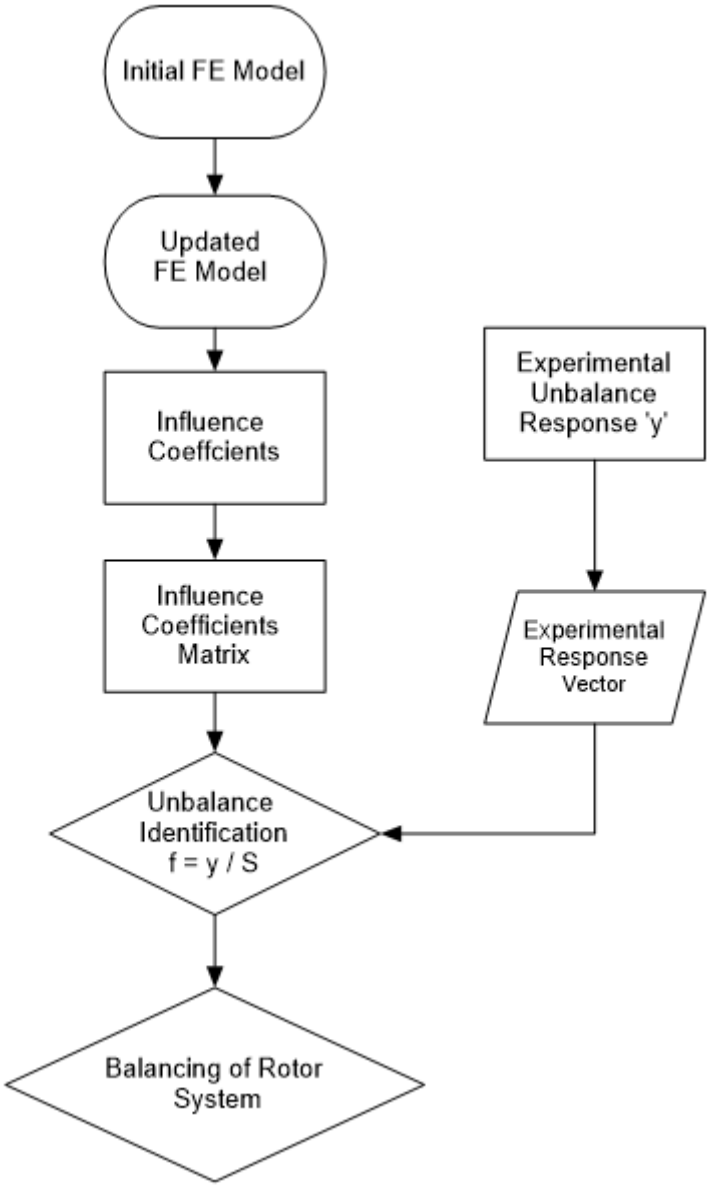

Figure 2 Flow chart for unbalance identification

4 Experimental Setup and Finite element model

4.1 Setup for the Experiment Work

Figure 3 shows the results of the experimental examination of the equipment, which employed a Spectra Quest Machinery Fault Simulator Lite. A spiral coupling was used to drive the shaft, which was attached to a variable-speed motor. In order to determine natural frequencies and compute the Frequency Response Function (FRF), data was collected from vibration signals using a real-time data analyser (OROS OR34). The data was then processed using NVGate-11 software. During the impact test, an accelerometer (PCB PIEZOTRONICS, model 352C33, sensitivity 10.19 mV/m/s^2) was used to evaluate the vibration responses of the stationary shaft. With a sensitivity of 1.156 mV/N, the ENDEVCO model 2302-5 modal hammer was used to stimulate the shaft. Furthermore, the phase angle and imbalance response were ascertained by means of a signal conditioner and two proximity probes, the former of which had a sensitivity of 4.73 V/mm and the latter of which had a range of 0-2 mm, both produced by Spectra Quest.

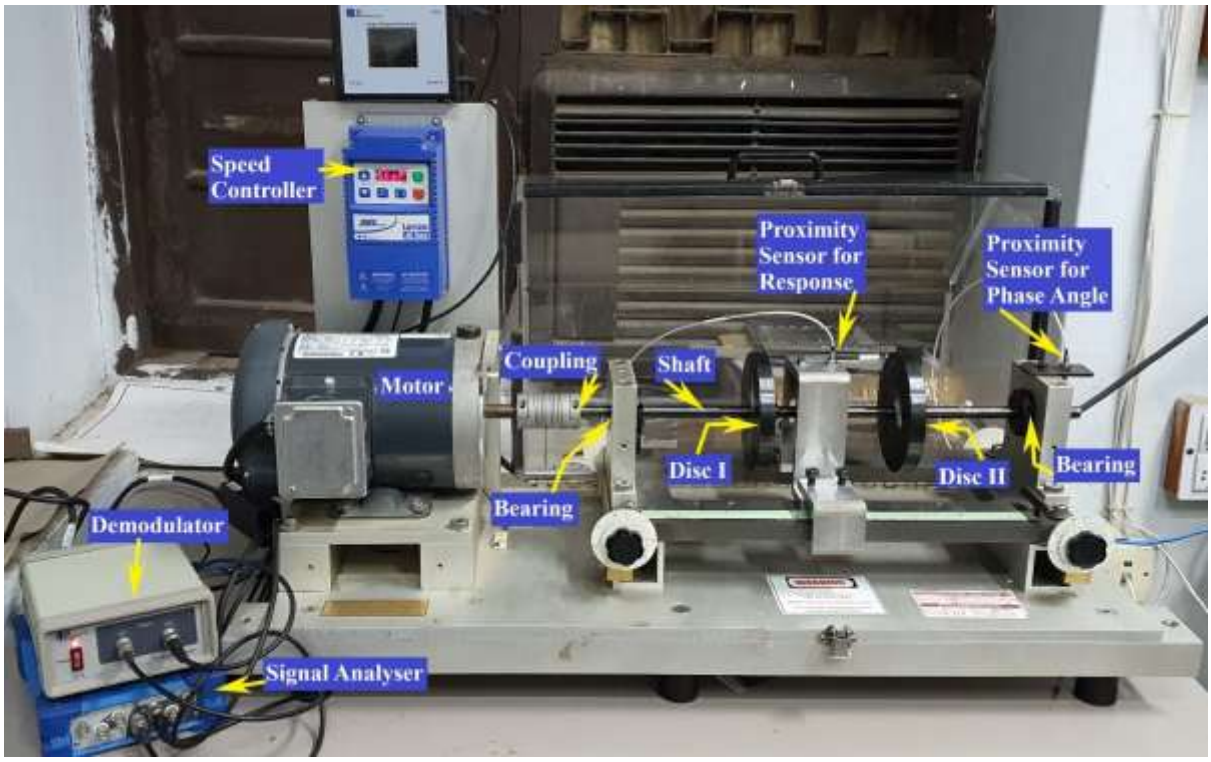

Figure 3 Experimental Setup

The rotor shaft system is shown in Figure 4 in which bearings are modelled as combination of spring damper arrangement. Two discs both of 126 mm in diameter and 15.3 mm thickness are mounted on the shaft of 13 mm diameter and 430 mm length. The disc I and disc II are located at equal distance of 143.3 mm from left and right bearing respectively and the distance between the two disc is also 143.3 mm.

The shaft and disc material possess a density of 7800 kg/m^3, a Young's modulus of 210 MPa, and a Poisson's ratio of 0.3. The disc has the following inertial properties: mass =

1.412 kg, polar moment of inertia (Ixx) = 2784.324 kg·mm^2, and diametral moments of inertia (Iyy = Izz) = 1422.338 kg·mm^2.

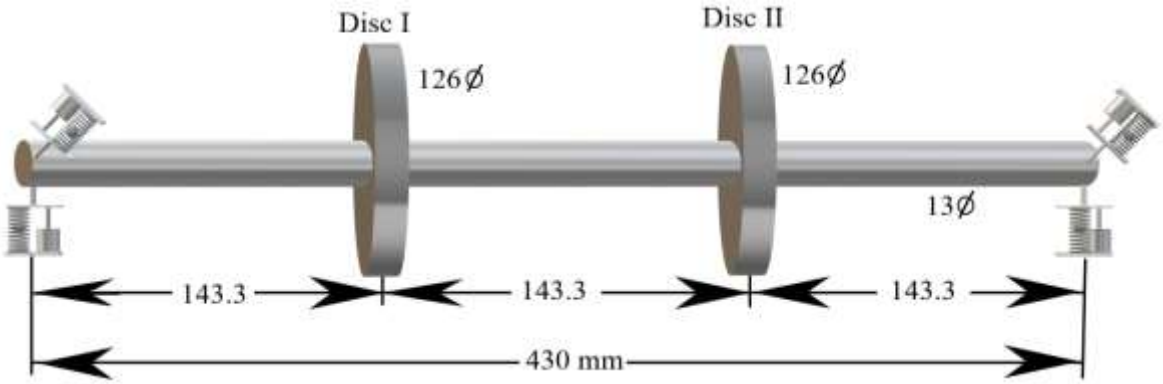

Figure 4 The rotor system considered

4.2 Finite Element Model

Figure 5 illustrates a depiction of the finite element mesh model of the rotor bearing system. This research employs a finite element model to ascertain the influence coefficients, which are then applied in the approach for diagnosing the imbalance. The shaft has been discretised into 48 equal-length, two-node Timoshenko beam elements to account for shear deformation. The bearing points are represented by nodes 1 and 49 in this discretisation. Figure 1 depicts the degrees of freedom associated with the examined beam element. The rotor system's disc is modelled as a point mass in the finite element analysis. This is achieved by considering the characteristics of inertia.

Figure 5 F E Mesh and response measurement points

To keep the rotor system in place, ball bearings are located at the shaft's two ends. The two bearing supports have been simulated with radial and torsional stiffness and isotropic damping coefficients. Originally proposed for the FE model are the following damping coefficients and bearing stiffness values [30, 31];

Stiffness in mutually perpendicular radial directions **y** and **z** is 1 x 10^8 N/m, similarly damping in radial **y** and **z** direction 200 Ns/m, torsional stiffness about **y** and **z** is 1 x 10^6 Nm/rad and torsional damping about **y** and **z** is 10 Nm s / rad for left- and right-hand side bearings.

The initial FE model is thus prepared using the mentioned inertial, stiffness, and damping values. Before using the first FE model to find the effect coefficients for imbalance detection, it is important to make sure it is correct.

4.3 Updating the Finite Element Model

If the FE model used to calculate the Influence Coefficient is of not correct, then the FE model-based approach for imbalance identification will not be accurate. Consequently, in order to detect imbalance, the FE model of the rotor system must be revised. The FE model is updated using the MATLAB-created inverse eigen sensitivity method (IESM) [32], which is based on the work of Chouksey (2012) and Chouksey, et al. (2013). In order to update the system's finite element model, the IESM finite element model updating technique makes use of the measured eigen data. The rotor model is updated using the experimental natural frequencies and damping factor for the first four bending modes.

Shaft stiffness, disc and shaft inertia, Young's modulus, Poisson's ratio, and shaft material density are all taken into account while modelling the rotor system. Additionally, bearing stiffness and bearing damping coefficient in both radial and angular directions are taken into account when updating the model. Updates to the bearing parameters are made iteratively using the finite element model updating procedure. Figure 6 displays the cumulative correction factor versus the number of iterations. After 20 iterations, it is evident that the updating parameters are convergent.

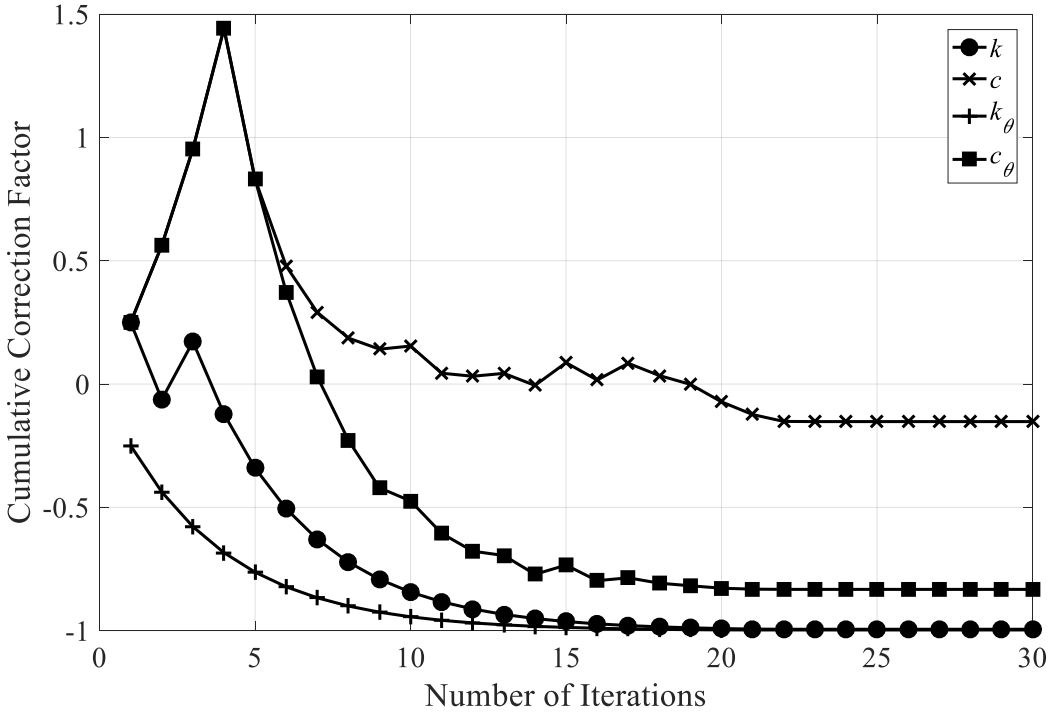

Figure 6 Cumulative correction factor vs number of iterations

The updated stiffness and damping properties of bearings are mentioned below;

Radial stiffness	$K_{yy}^{L} = K_{zz}^{R} = K_r$ = 5.9 x 10^5 N/m
Radial damping	$C_{yy}^{L} = C_{zz}^{R} = K_r$ = 170 Ns/m
Torsional stiffness	$K^{L}{}_{\theta yy} = K^{R}{}_{\theta zz} = K_\theta$ = 3.1257 x 10^3 Nm/rad
Torsional damping	$C^{L}{}_{\theta yy} = C^{R}{}_{\theta zz} = C_\theta$ = 1.7 Nm s / rad

Bearing stiffness and damping is represented by *k* and *c* respectively. Superscript L and R are used for left and right bearing respectively. The symbol θ is for tortional direction.

The natural frequencies determined from the experiment and updated FE model are given in the Table 1.

Table 1 Natural Frequencies

S No.	Natural Frequency from experiment (Hz)	Natural Frequency from FE Model (Hz)
1.	51	54.24
2.	53	54.24
3.	141	142.88
4.	144	143.14

Figure 7 (a) shows the percentage inaccuracy as a function of the number of repetitions in the natural frequency, whereas Figure 7 (b) shows the modal damping factor for the first four bending modes. The isotropic design of the bearing explains why the percentage error variations in the first two modes and the third and fourth modes are superimposed. After 25 rounds of convergence, the modal damping factor and natural frequency error are reduced.

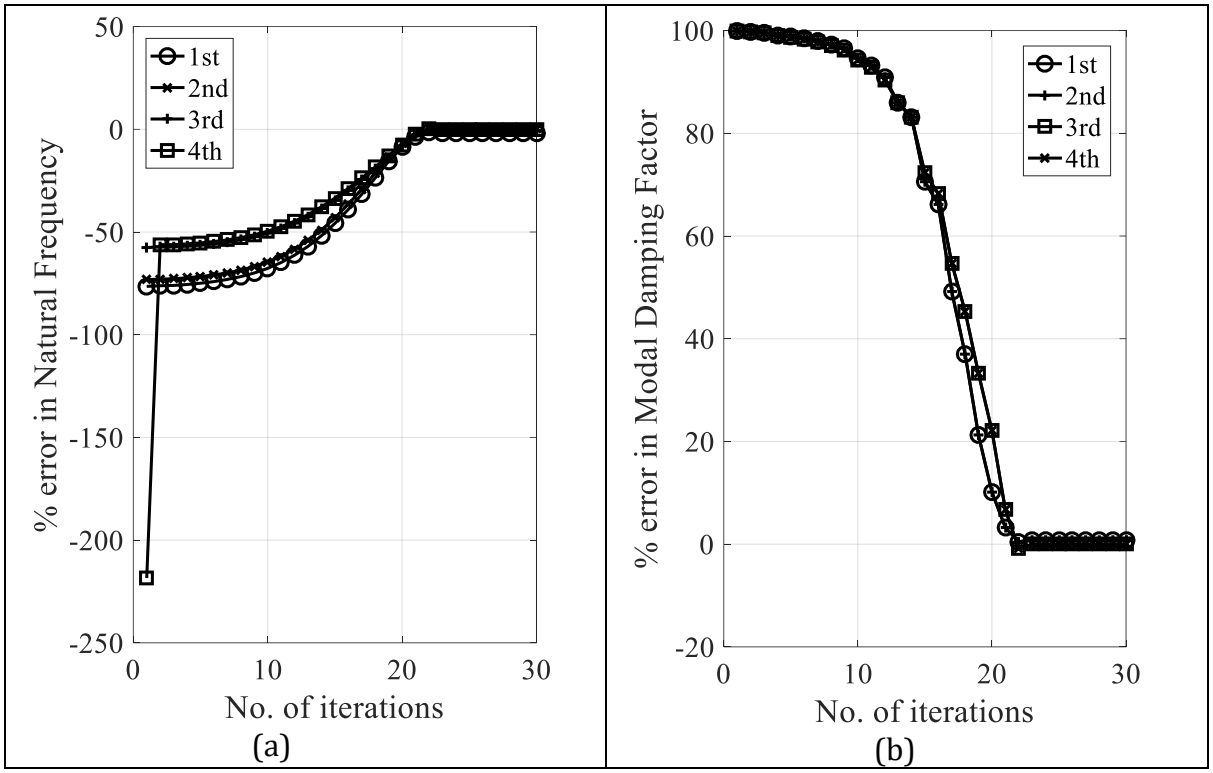

Figure 7 Percentage error against no. of iterations for (a) natural frequencies, (b) modal damping factors

4.4 Whirl speed map

In order to visually identify crucial rotation speeds, researchers often utilise Campbell diagrams, which are also called Whirl Speed Maps, to examine the relationship between natural frequencies and spin speed. The Campbell diagram for the two-disc rotor system, which was obtained using the revised FE model, is shown in Figure 8. The figure illustrates the forward and backward spin variations of the first three bending modes. In the first forward direction (1F) and first backward direction (1B), there is a minute gyroscopic split, however in the second forward direction (2F) and second backward direction (2B), there is slightly greater divide. There is a clear division between third forward (3F) and third backward (3B) on the charts depicting the gyroscopic effect intensity in this mode. Along with the three bending modes, a torsion (1T) is also appearing between the second and third bending modes. At the point where the Synchronous Whirl Line (SWL) and the first forward mode (1F) dashed line meet, the graphic, visible in enlarged view, encircles the first crucial speed in red. The illustration indicates that 3228 RPM is the essential speed.

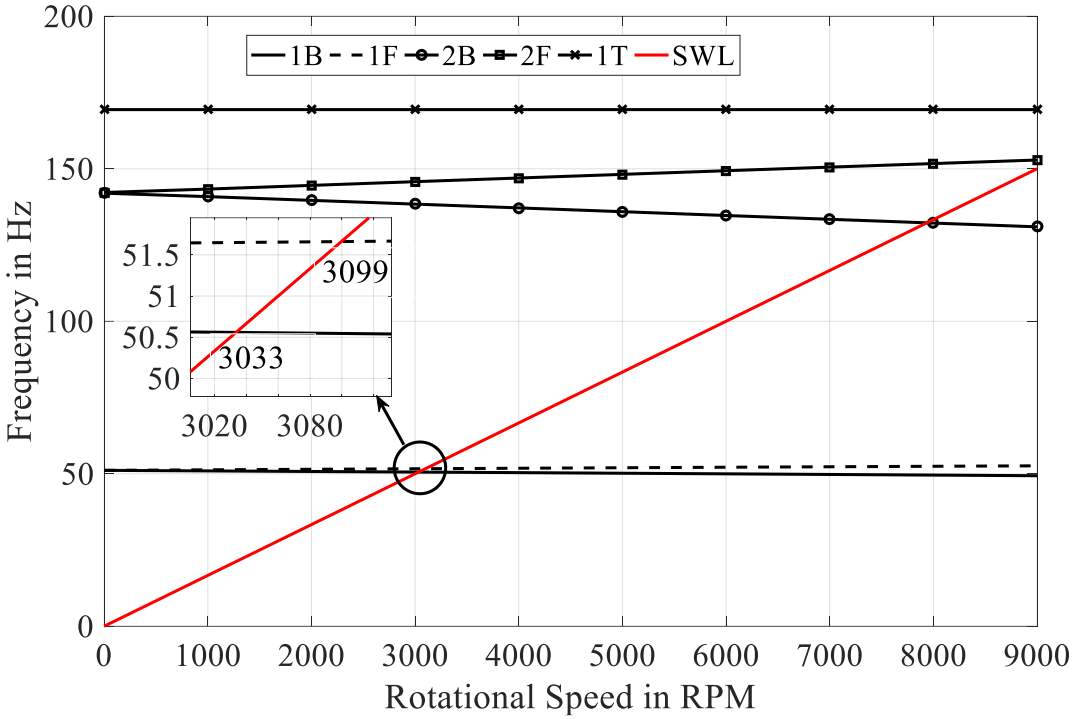

Figure 8 Whirl speed map

5 Influence Coefficient and Unbalance Response

The updated FE model created in Section 4.2 is used to calculate the rotor system's influence coefficient, which is then utilised to create the influence coefficient matrix. Unbalance responses are taken from the MFS experimental setup as described in the Section 4.1.

5.1 Influence Coefficient

Influence Coefficient analysis may be useful in the unbalance identification as it reveals the influence coefficients. Such an analysis may be helpful in proper selection of measurement points [34]. In this work, the unbalance has been considered in the two discs, i.e. disc I and disc II. Referring to the Figure 5, disc I is at node 18 and disc II is at node 34. Influence coefficients have been computed at nodes *i* = 10, 25 and 41which are at 71.6 mm, 215 mm and 358.3 mm from left bearing respectively by applying unit rotating unbalance forces at disc I (*j=18*) and disc II (*j=33*), one by one. These values have been listed in the Table 2 below at 900 RPM.

Table 2 Influence Coefficient at 900 RPM

	$S_{10\text{-}18}$	$S_{10\text{-}33}$	$S_{25\text{-}18}$	$S_{25\text{-}33}$	$S_{41\text{-}18}$	$S_{41\text{-}33}$
Influence Coefficient in m / kg m	4.91×10^{-2} $\angle 5.4^{o}$	3.42×10^{-2} $\angle 5.4^{o}$	7.05×10^{-1} $\angle 5.4^{o}$	7.05×10^{-1} $\angle 5.4^{o}$	3.42×10^{-2} $\angle 5.4^{o}$	4.91×10^{-2} $\angle 5.4^{o}$

5.2 Unbalance response

Unbalance force of 5.79×10^{-2} kg-m is applied on disc I and 6.31×10^{-2} kg-m disc II at different angular position from a reference position. Responses are taken using proximity sensor at node number 10, 25 and 41 and angle of response is also recorded with help of a proximity sensor used as keyphasor. The responses at different locations are recorded with angles and the same is shown in Table 3 below.

Table 3 Unbalance responses at various points at 900 RPM

UB at angle		Response locations	Response at angle
Disc I	Disc II		
$5.79\times10^{-4}\angle0^{o}$	$6.31\times10^{-4}\angle0^{o}$	y_{10}	$5.05\times10^{-5}\angle5.4^{o}$
		y_{25}	$8.54\times10^{-5}\angle5.4^{o}$
		y_{41}	$5.10\times10^{-5}\angle5.4^{o}$
$5.79\times10^{-4}\angle0^{o}$	$6.31\times10^{-4}\angle30^{o}$	y_{10}	$5.01\times10^{-5}\angle19^{o}$
		y_{25}	$8.53\times10^{-5}\angle21^{o}$
		y_{41}	$5.21\times10^{-5}\angle22^{o}$
$5.79\times10^{-4}\angle0^{o}$	$6.31\times10^{-4}\angle60^{o}$	y_{10}	$4.70\times10^{-5}\angle34^{o}$
		y_{25}	$8.53\times10^{-5}\angle38^{o}$
		y_{41}	$4.75\times10^{-5}\angle43^{o}$
$5.79\times10^{-4}\angle30^{o}$	$6.31\times10^{-4}\angle30^{o}$	y_{10}	$5.04\times10^{-5}\angle36^{o}$
		y_{25}	$8.59\times10^{-5}\angle36^{o}$
		y_{41}	$5.21\times10^{-5}\angle36^{o}$
$5.79\times10^{-4}\angle30^{o}$	$6.31\times10^{-4}\angle60^{o}$	y_{10}	$4.69\times10^{-5}\angle49^{o}$
		y_{25}	$8.41\times10^{-5}\angle51^{o}$
		y_{41}	$4.63\times10^{-5}\angle52^{o}$
$5.79\times10^{-4}\angle60^{o}$	$6.31\times10^{-4}\angle60^{o}$	y_{10}	$4.71\times10^{-5}\angle64^{o}$
		y_{25}	$8.32\times10^{-5}\angle64^{o}$
		y_{41}	$4.81\times10^{-5}\angle64^{o}$

A known unbalance is applied at 900 RPM and response is measured at node 10 and plotted with keyphasor response is plotted as shown in Figure 9. The introduced unbalance on disc I is $5.79\times10^{-2}\angle30^{o}$ kg-m and that on disc II is $6.31\times10^{-2}\angle30^{o}$ kg-m. The values of the unbalance responses node 10 found out to be as $9.93\times10^{-5}\angle36^{o}$ m.

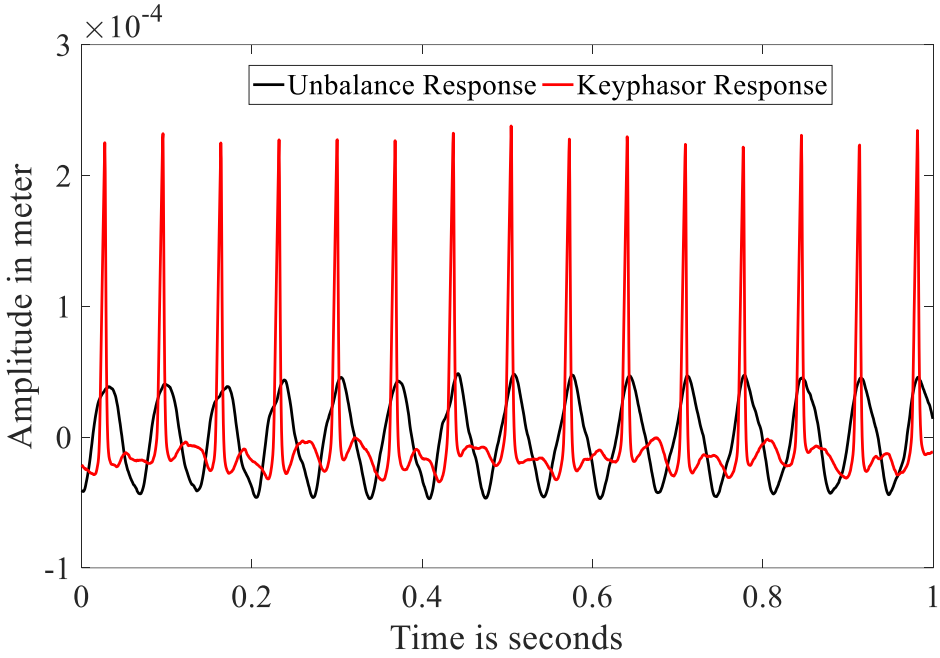

Figure 9 Rotor unbalance and keyphasor response at node 10 with unbalance at 30° on disc I and disc II

6 Unbalance Identification

The Influence Coefficient of the rotor system given in Table 2 in section 5.1 is used for the formation of Influence Coefficient matrix using Eqn. 3. The response vectors are formed using unbalance responses recorded in Table 3 by employing Eqn. 4. The unbalance force is determined applying Eqn. 7 and the same is tabulated in Table 4. Second and third column shows unbalance applied with angular position, fourth and fifth column shows identified unbalance and angular position and last two columns gives residual unbalance after balancing. The machine on which study is conducted is considered to be of machine tool drive or steam/gas turbine for which a balancing grade of G2.5 is applicable [35]. The rotor is rotational speed is kept 900 rpm and at this speed allowable residual unbalance as per balancing grade of G2.5 is 79.58 g mm.

Table 4 Identified Unbalance and Error in unbalance

S. No.	Introduced Unbalance on disc I 5.79×10^{-4} in kg-m	Introduced Unbalance on disc II 6.31×10^{-4} in kg-m	Identified Unbalance on disc I in kg-m	Identified Unbalance on disc II in kg-m	Residual UB g mm	Residual UB g mm
1.	$\angle0^{o}$	$\angle0^{o}$	$5.89\times10^{-4}\angle0^{o}$	$6.24\times10^{-4}\angle0^{o}$	10	7

2.	$\angle 0^o$	$\angle 30^o$	$5.46\times10^{-4}\angle 5.9^o$	$6.85\times10^{-4}\angle 22.9^o$	33	54
3.	$\angle 0^o$	$\angle 60^o$	$6.22\times10^{-4}\angle 9.3^o$	$6.51\times10^{-4}\angle 55.2^o$	43	20
4.	$\angle 30^o$	$\angle 30^o$	$5.55\times10^{-4}\angle 30.6^o$	$6.67\times10^{-4}\angle 30.6^o$	24	36
5.	$\angle 30^o$	$\angle 60^o$	$6.05\times10^{-4}\angle 37.6^o$	$5.91\times10^{-4}\angle 53.6^o$	26	40
6.	$\angle 60^o$	$\angle 60^o$	$5.48\times10^{-4}\angle 58.6^o$	$6.16\times10^{-4}\angle 58^o$	31	15

It can be observed that residual unbalance in different cases is below the permissible residual unbalance in both the disc.

7 Conclusions

Finding imbalance in multidisc rotor systems has been proposed using a finite element model technique. In a multi-disc rotor system where the imbalance force may be located at different angles, the proposed method has been usefully shown in experimental investigations. The main benefit of the suggested technique is that it reduces the amount of experimental trial runs required, which is three in conventional balancing approaches and two in the suggested way. However, before using this procedure again, you must verify that the finite element model is valid. Reducing the need for an actual trial run, the finite element model may be used to calculate the Influence Coefficient once the correctness of the model has been confirmed using the collected vibration data. In terms of both the disc rotor system and its angular position, the testing results show that the suggested method accurately identifies disc imbalance. The proposed method supposedly finds imbalances quickly and effectively.

References

[1] A. Muszynska, *Rotor dynamics*, 2005 ed. CRC Press, Taylor and Francis 2005.
[2] J. S. Rao, A note on jeffcott warped rotor, *Mech Mach Theory,* vol. 36, pp. 563-575, 2001.
[3] M. I. Friswell, J. E. T. Penny, S. D. Garvey, and A. W. Lees, *Dynamics of Rotating Machines* (Cambridge Aerospace Series). New York: Cambridge University Press, p. 526, 2010.
[4] A. Shrivastava and A. R. Mohanty, Identification of unbalance in a rotor system using a joint input-state estimation technique, *J Sound Vib,* vol. 442, pp. 414-427, 2019.
[5] R. P. Fabio Dalmazzo Sanches, Simultaneous identification of unbalance and shaft bow in a two-disk rotor based on correlation analysis and the SEREP model order reduction method, *J Sound Vib,* vol. 433 pp. 230-247, 2018.
[6] J. Yao, L. Liu, F. Yang, F. Scarpa, and J. Gao, Identification and optimization of unbalance parameters in rotor-bearing systems, *J Sound Vib,* vol. 431, pp. 54-69, 2018.
[7] J. S. Rao, *Rotor dynamics*, 3rd ed. New age international (P) Ltd, 1996.
[8] G. Genta, *Dynamics of rotating systems*, 2005 ed. (Mechanical Engineering Series). Springer, 2005.
[9] D. Norfield, *Practical balancing of rotating machinery*, First edition 2006 ed. Elsevier, 2006.
[10] R. Tiwari, *Rotor systems: analysis and identification*, 2017 ed. CRC Press, 2017.
[11] P. Gneilka, Modal balancing of flexible rotors without test runs: an experimental investigation, *Journal of Vibration and Acoustics,* vol. 90, pp. 157–172, 1983.

[12] T. Kreuzinger-Janik and H. Irretier, Experimental modal analysis - a tool for unbalance identification of rotating machines, *Int J Rotating Mach,* vol. 6, no. 1, pp. 11-18, 2000.
[13] D.-J. Han, Generalized modal balancing for non-isotropic rotor systems, *Mech Syst Signal Process,* vol. 21, no. 5, pp. 2137-2160, 2007.
[14] M. S. Darlow, A. J. Smalley, and A. G. Parkinson, Demonstration of a unified approach to the balancing of flexible rotors, *J Eng P,* vol. 103, pp. 101-107, 1981.
[15] S. G. Tan and X. X. Wang, A theoritial introduction to low speed balancing of flexible rotors: unification and development of the modal balancing and influence coefficient techniques, *J Sound Vib,* vol. 168(3), pp. 385-394, 1993.
[16] E. S. Zorzi, C. C. Lee, and J. C. Giordano, Developement and Application of a Unified Balancing Approach with Muliple Constraint.
[17] J. K. Sinha, A. W. Lees, and M. I. Friswell, Estimating unbalance and misalignment of a flexible rotating machine from a single run-down, *J Sound Vib,* vol. 272, pp. 967–989, 2004.
[18] R. Markert, R. Platz, and M. Seidler, Model based fault identification in rotor systems by least squares fitting, *Int J Rotating Mach,* vol. 7, no. 5, pp. 311-321, 2001.
[19] A. W. Lees, J. K. Sinha, and M. I. Friswell, Model based identification of rotating machines, *Mech Syst Signal Process,* vol. 23, pp. 1884-1893, 2009.
[20] A. K. Jalan and A. R. Mohanty, Model based fault diagnosis of a rotor-bearing system for misalignment and unbalance under steady-state condition, *J Sound Vib,* doi: 10.1016/j.jsv.2009.07.014 vol. 327, no. 3-5, pp. 604-622, 2009.
[21] A. S. Sekhar, Crack identification in a rotor system:a model-based approach, *J Sound Vib,* vol. 270, pp. 887-902, 2003.
[22] J. R. Jain and T. K. Kundra, Model based online diagnosis of unbalance and transverse fatigue crack in rotor systems, *Mech Res Commun,* vol. 31, pp. 557-568, 2004.
[23] G. N. D. S. Sudhakar and A. S. Sekhar, Identification of unbalance in a rotor bearing system, *J Sound Vib,* vol. 330, pp. 2299-2313, 2010.
[24] Z. X. Zhang, Q. Zhang, X. L. Li, and T. L. Qian, The whole-beat correlation method for the identificationofan unbalance response of a dual-rotor system with a slight rotating speed difference, *Mech Syst Signal Process,* vol. 25, pp. 1667–1673, 2010.
[25] R. M. Furtado, K. L. C. Dedini, P. Pennacchi, and V. L. Jr., Fault identification in rotor system using model based methods, experimental data and artificial neural network, in *18th International Congress of Mechanical Engineering*, Ouro Preto, MG, 2005.
[26] J. McBain and M. Timusk, Fault detection in variable speed machinery : Statistical parameterization, *Journal ofSoundandVibration,* vol. 327, pp. 623-646, 2009.
[27] J. K. Sinha and K. Elbhbah, A future possibility of vibration based condition monitoring of rotating machines, *Mech Syst Signal Process,* vol. 34, pp. 231–240, 2012.
[28] K. Elbhbah and J. K. Sinha, Vibration-based condition monitoring of rotating machines using a machine composite spectrum, *J Sound Vib,* vol. 332, pp. 2831–2845, 2013.
[29] I. Chatzisavvas and F. Dohnal, Unbalance identification using the least angle regression technique, *Mech Syst Signal Process,* vol. 50-51 no. 706–717, 2014.
[30] M. Chouksey, J. K. Dutt, and S. V. Modak, Model updating of rotors supported on ball bearings and its application in response prediction and balancing, *Measurement,* vol. 46, no. 10, pp. 4261-4273, 2013.
[31] Dinesh Kumar Pasi, Manoj Chouksey, and A. Tiwari, A finite element model-based approach for rotor unbalance detection and balancing, *Journal of The Institution of Engineers (India): Series C* vol. 104, pp. 479-494, 2023.
[32] MATLAB Version 9.9.0.157001 (R2020b) Natick, Massachusetts,The MathWorks Inc.2020
[33] M. Chouksey, Studies in modal analysis, frequency response characteristics and finite element model updating of rotor systems, *Ph D,* no. TH-4224, p. 237, 2012.
[34] D. K. Pasi, M. Chouksey, and A. K. Gupta, Sensitivity Analysis for Unbalance Identification of Rotor Systems, presented at the National Symposium on Rotor Dynamics (NSRD) 2019, Bangalore, 2019.

[35] *ISO 1940-1:2003 (2003) Mechanical vibration - Balance quality requirements for rotors in a constant (rigid) state- Part 1: Specification and verification of balance tolerances*, 2003.